GEOPHYSICS, VOL. 83, NO. 3 (MAY-JUNE 2018); P. M1–M13, 13 FIGS., 4 TABLES.
10.1190/GEO2017-0364.1

Bayesian linearized petrophysical AVO inversion

Xiaozheng Lang[1] and Dario Grana[1]

ABSTRACT

Seismic reservoir characterization aims to provide a 3D model of rock and fluid properties based on measured seismic data. Petrophysical properties, such as porosity, mineral volumes, and water saturation, are related to elastic properties, such as velocity and impedance, through a rock-physics model. Elastic attributes can be obtained from seismic data through seismic modeling. Estimation of the properties of interest is an inverse problem; however, if the forward model is nonlinear, computationally demanding inversion algorithms should be adopted. We have developed a linearized forward model, based on a convolutional model and a new amplitude variation with offset approximation that combined Gray's linearization of the reflectivity coefficients with Gassmann's equation and Nur's critical porosity model. Physical relations between the saturated elastic moduli and the matrix elastic moduli, fluid bulk modulus, and porosity are almost linear, and the model linearization can be obtained by computing the first-order Taylor series approximation. The inversion method for the estimation of the reservoir properties of interest is then developed in the Bayesian framework. If we assume that the distributions of the prior model and error term are Gaussian, then the explicit analytical solution of the posterior distribution of rock and fluid properties can be analytically derived. Our method has first been validated on synthetic seismic data and then applied to a 2D seismic section extracted from a real data set acquired in the Norwegian Sea.

INTRODUCTION

The goal of seismic reservoir characterization is to provide an accurate description of the subsurface properties in the target interval. The process of transforming the measured geophysical data, for example, seismic or electromagnetic data, into physical properties of porous rocks is an inverse problem (Tarantola, 2005; Doyen, 2007; Sen and Stoffa, 2013). Generally, seismic inversion aims to transform reflection seismic data into elastic properties, such as impedance, seismic velocity, or elastic moduli (Aki and Richards, 1980; Oldenburg et al., 1983; Russell, 1988; Sen and Stoffa, 2013), and the estimation of petrophysical attributes from measured data consists of seismic inversion and rock-physics (or petrophysics) inversion (Mukerji et al., 2001; Coléou et al., 2005; Doyen, 2007; Gunning and Glinsky, 2007; Bosch et al., 2010; Grana and Della Rossa, 2010; Rimstad and Omre, 2010; Kemper and Gunning, 2014; Connolly and Hughes, 2016; Jullum and Kolbjørnsen, 2016; Grana et al., 2017).

The seismic forward model is the process of converting the subsurface geologic elastic properties into the corresponding seismic response. These models can be simple equations, such as convolutional models, or more complex methods, such as elastic wave propagation. Convolutional models introduce some approximations in the data prediction, and the underlying assumptions, such as plane reflectors and weak elastic contrasts, are valid only for a limited subset of geologic scenarios; however, full-waveform propagation provides a more accurate physical description of the elastic response, but the corresponding inversion methods are more computationally demanding due to the complexity of the forward model (Sayers and Chopra, 2009). Rock-physics models aim to transform petrophysical properties, such as porosity, mineral volumes, and water saturation, into a set of elastic variables (Avseth et al., 2005; Mavko et al., 2009; Dvorkin et al., 2014). These models generally consist of a set of physical equations, such as empirical multivariate linear regressions (Han, 1986) or complex poroelastic relations (Mavko et al., 2009), and relate elastic moduli or velocities to rock and fluid properties. Generally, the choice of rock-physics model depends on the specific sedimentary environment.

In this work, we propose a new linearized forward model based on the amplitude variation with offset (AVO) approximation and the linearized rock-physics model. The linearization of the seismic

Manuscript received by the Editor 9 June 2017; revised manuscript received 12 December 2017; published ahead of production 11 January 2018; published online 27 March 2018; corrected version published online 27 March 2018.
[1]University of Wyoming, Department of Geology and Geophysics, Laramie, Wyoming, USA. E-mail: xlang@uwyo.edu.

forward model based on the convolution of the seismic wavelet and the linearized approximation of Zoeppritz equations is commonly used in seismic inversion (Aki and Richards, 1980; Russell, 1988; Gray et al., 1999). The linearization of the rock-physics model is less common in reservoir characterization. The relation between elastic properties and rock properties, such as porosity and mineral volumes, is generally close to being linear. However, the relation between water saturation and saturated-rock elastic properties is generally nonlinear, especially when the fluid mixture is homogeneous. Ball et al. (2014) show that the nonlinearity is caused by the application of fluid-mixture laws and that the relations between the fluid bulk modulus and the saturated-rock bulk modulus is linear in Gassmann's equation. Gassmann's equation requires a model for the computation of the dry-rock bulk modulus. If we combine Gassmann's equation with Nur's critical model, we obtain a rock-physics model in which the saturated-rock bulk and shear moduli are almost linear with respect to porosity, matrix bulk and shear moduli, and fluid bulk modulus. When the physical model is almost linear, we can replace the exact equation with a linearized approximation computed by truncating the Taylor series expansion to the first order (Grana, 2016). By combining Gray's AVO approximation (Gray et al., 1999) with the linearized rock-physics model, we obtain a linearized seismic-petrophysical forward model, namely, linearized petrophysical AVO approximation. This work is presented for the rock-physics model combining Nur's and Gassmann's equations, for which the linearized approximation can be analytically computed; however, the methodology could be extended to other rock-physics equations by computing the Taylor series expansion using numerical expressions of the Jacobian of the rock-physics model. Linearized approximations are generally valid for rock-physics models that are almost linear, but they might fail for nonlinear models, such as the soft sand model, as discussed by Grana (2016).

Our linearized formulation of the forward model expresses the angle-dependent reflection coefficients as a function of six variables: porosity, matrix bulk modulus, matrix shear modulus, matrix density, fluid bulk modulus, and fluid density. This formulation can be used in an inverse problem setting to estimate rock and fluid properties from seismic data. If the number of angle stacks is small, the inverse problem is underdetermined and the solution is not necessarily unique; however, we point out that some of the model properties are strongly correlated (for example, the bulk and shear moduli of the matrix and the matrix density because they all depend on the mineral volumes, and the fluid bulk modulus and density because they both depend on water saturation), and such correlations can be used as additional constraints in the inversion to mitigate the nonuniqueness of the solution. In our approach, the linearized petrophysical AVO approximation is used to estimate the posterior distribution of rock and fluid properties in the reservoir in a Bayesian inversion framework.

Deterministic methods cannot capture the entire set of possible solutions, but they can provide a local minimum. Probabilistic algorithms, such as Bayesian inverse methods, are then preferable to solve ill-conditioned problems and to quantify the uncertainty of the model parameters (Gouveia and Scales, 1998; Ulrych et al., 2001; Buland and Omre, 2003; Tarantola, 2005; Grana and Della Rossa, 2010; Liu and Grana, 2017). Buland and Omre (2003) apply the Bayesian approach to elastic seismic inversion. Tjelmeland and Omre (1997) and Eidsvik et al. (2004) use Bayesian approaches to predict the spatial distribution of facies, whereas Buland and Kolbjørnsen (2012) apply a Bayesian inversion algorithm to estimate the resistivity model from electromagnetic data. Similar approaches were applied to predict petrophysical properties from seismic data (Grana and Della Rossa, 2010; Rimstad and Omre, 2010; Jullum and Kolbjørnsen, 2016; Grana et al., 2017). Common assumptions in Bayesian inversion include the linearization of the forward model and the Gaussian distribution of the prior model and the data-error term. Under these assumptions, the posterior distribution of the model parameters is Gaussian and can be expressed in a closed form. The analytical formulation can be extended to the Gaussian mixture case (Grana and Della Rossa, 2010; Grana et al., 2017). If the prior distribution of the model is not Gaussian distribution and/or the forward model is not linear, Monte Carlo methods can be applied to evaluate the posterior distribution of the model (Doyen and Den Boer, 1996; Sen and Stoffa, 1996, 2013; Bosch et al., 2010; Hammer et al., 2012). However, the application of these methods might be time consuming because of the high dimensions of model space.

We applied our method to a synthetic data set to test the validity of the approach and to a real data set, including well-log data and a 2D seismic section, of a hydrocarbon reservoir in the Norwegian Sea for a seismic reservoir characterization study.

METHODOLOGY

The prediction of rock and fluid properties from seismic data is generally obtained by combining seismic and rock-physics inversion. In this work, we propose a linearized model integrating a rock-physics model with a convolutional model based on the reflectivity method and use it in a Bayesian inverse approach.

The geophysical inverse problem can be written in the following form:

$$\mathbf{d} = \mathbf{f}(\mathbf{q}) + \boldsymbol{\varepsilon} = \mathbf{f}(\mathbf{g}(\mathbf{m})) + \boldsymbol{\varepsilon}, \tag{1}$$

where $\mathbf{d}$ represents the seismic data, $\mathbf{q}$ is the elastic attributes, $\mathbf{m}$ is the reservoir properties, $\boldsymbol{\varepsilon}$ is the data error term, $\mathbf{f}$ is the seismic model linking the seismic data $\mathbf{d}$ to the elastic attributes $\mathbf{q}$, and $\mathbf{g}$ is the rock-physics model linking the elastic attributes $\mathbf{q}$ to the reservoir properties $\mathbf{m}$.

In seismic-petrophysics inversion, the model parameters include the reservoir properties of interest $\mathbf{m}$, such as porosity, as well as rock and fluid properties. In general, the forward models $\mathbf{f}$ and $\mathbf{g}$ are nonlinear. In the following subsections, we propose a linearization of the joint forward models and apply it in a Bayesian inverse approach.

Forward model: Seismic model

For the linearization of the seismic forward model, we adopt a linear operator based on the convolution between the seismic wavelet and the reflection coefficients:

$$\mathbf{d} = \mathbf{W}\boldsymbol{r}_{\mathbf{pp}} + \boldsymbol{\varepsilon}, \tag{2}$$

where $\mathbf{W}$ represents a matrix associated with the wavelet, $\boldsymbol{r}_{\mathbf{pp}}$ represents the reflection coefficient series that is a function of the elastic properties $(\mathbf{q})$ across the interfaces, and $\boldsymbol{\varepsilon}$ is the error term. In an isotropic elastic medium, under the assumption of small

elastic contrasts across the reflecting interface, the reflection coefficient can be approximated by a sum of three terms that depend on P- and S-wave velocities and density (Aki and Richards, 1980). Stolt and Weglein (1985) extend Aki-Richards equation to the time-continuous case:

$$r_{pp}(t,\theta) = \frac{1}{2}(1+\tan^2\theta)\frac{\partial}{\partial t}\ln\, V_P(t) - 4\frac{1}{\gamma^2}\sin^2\theta\frac{\partial}{\partial t}\ln\, V_S(t) + \frac{1}{2}\left(1-4\frac{1}{\gamma^2}\sin^2\theta\right)\frac{\partial}{\partial t}\ln\rho_{sat}(t), \quad (3)$$

where θ is the incident angle, $V_P(t)$ and $V_S(t)$ are the P- and S-wave velocities at a given time t, and γ is the V_P/V_S ratio. Various formulations of equation 3 have been proposed (Russell et al., 2011). The AVO approximation based on Gray et al. (1999) is the most suitable for the joint seismic-petrophysics inversion because it relates the reflection coefficients to the saturated-rock elastic moduli and density as

$$r_{pp}(t,\theta) = \left(\frac{1}{4}-\frac{1}{3\gamma^2}\right)\sec^2\theta\frac{\partial}{\partial t}\ln\, K_{sat}(t) + \frac{1}{\gamma^2}\left(\frac{\sec^2\theta}{3}-2\sin^2\theta\right)\frac{\partial}{\partial t}\ln\, G_{sat}(t) + \left(\frac{2-\sec^2\theta}{4}\right)\frac{\partial}{\partial t}\ln\rho_{sat}(t), \quad (4)$$

where K_{sat}, G_{sat}, and ρ_{sat} are the saturated-rock bulk modulus, shear modulus, and density, respectively.

Forward model: Rock-physics model

The rock-physics model generally links the reservoir properties of interest to the saturated-rock bulk modulus, shear modulus, and density. In our work, the rock-physics model includes Gassmann's equation and Nur's critical porosity model (Mavko et al., 2009). Gassmann's equation assumes that the porous material is isotropic and homogeneous and that the pore space is connected and in pressure equilibrium (Berryman, 1999; Mavko et al., 2009) and is used to estimate the fluid effect of the elastic moduli when the porosity, the elastic moduli of dry rock, and the elastic moduli of the solid and fluid phases are known:

$$K_{sat} = K_{dry} + \frac{2}{\frac{\phi}{K_{fl}} + \frac{1-\phi}{K_m} - \frac{K_{dry}}{K_m^2}}, \quad (5)$$

where K_{sat} is the saturated-rock bulk modulus, K_{dry} is the dry-rock bulk modulus, K_m is the matrix bulk modulus, K_{fl} is the fluid bulk modulus, and ϕ is the porosity. Gassmann's model also assumes that the saturated-rock shear modulus G_{sat} is not affected by the pore fluids:

$$G_{sat} = G_{dry}, \quad (6)$$

where G_{dry} is the dry-rock bulk modulus. The elastic moduli of the solid and fluid phases depend on the mineral volumes and fluid saturations. Dry-rock elastic moduli are either measured in the laboratory (Murphy, 1984) or are computed by theoretical rock-physics models (Mavko et al., 2009; Russell, 2013; Dvorkin et al., 2014). A common model to estimate the dry-rock elastic moduli is Nur's critical porosity equation (Nur, 1992; Mavko and Mukerji, 1995), where the dry-rock elastic moduli are expressed as linear functions of porosity, with the coefficients of the linear regression depending on the matrix elastic moduli, K_m and G_m, and the critical porosity ϕ_0:

$$K_{dry} = K_m\left(1-\frac{\phi}{\phi_0}\right), \quad (7)$$

$$G_{dry} = G_m\left(1-\frac{\phi}{\phi_0}\right). \quad (8)$$

The saturated-rock density ρ_{sat} is generally computed as a linear combination of the matrix density ρ_m and the fluid density ρ_{fl} weighted by the solid and pore-space volume, respectively:

$$\rho_{sat} = \rho_m(1-\phi) + \rho_{fl}\phi. \quad (9)$$

By combing Gassmann's equation, Nur's critical porosity model, and the density equation, we obtain a system of rock-physics equations that links the elastic properties (K_{sat}, G_{sat}, and ρ_{sat}) in equation 4 to the reservoir properties of interest ($K_m, G_m, \rho_m, K_{fl}, \rho_{fl}$, and ϕ). The elastic moduli and density of the matrix depend on the mineral composition of the solid phase of the porous rock. Similarly, the bulk modulus and density of the fluid depend on the composition of the pore fluid. In Figure 1a, we show that the physical relation between K_m and K_{sat} is almost linear. The solid black lines represent the exact rock-physics model, and the dotted red lines represent the linear approximation. For the shear modulus and density, equations 6 and 8 show that G_{sat} is linear with respect to G_m, and equation 9 shows that ρ_{sat} is linear with respect to ρ_m. Therefore, we conclude that the linearization of the saturated-rock elastic properties in terms of the matrix elastic properties provide accurate results, as proven by

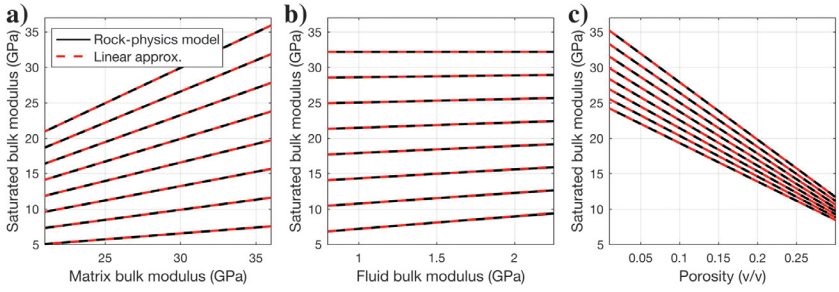

Figure 1. Numerical comparison of the exact rock-physics model (solid black lines) and the linear approximation (dotted red lines) obtained by first-order Taylor's series approximation. (a) Saturated bulk modulus versus rock matrix bulk modulus (each line refers to a porosity value; the porosity varies from 0 to 0.35; the water saturation is constant), (b) saturated bulk modulus versus fluid bulk modulus (each line refers to a porosity value; the porosity varies from 0 to 0.35; the mineral volumes are constant), (c) saturated bulk modulus versus porosity (each line refers to a matrix bulk modulus; the matrix bulk modulus varies from 24 to 36 GPa, corresponding to a variation in clay volume from 0.75 to 0; the water saturation is constant).

laboratory experiments (Mavko et al., 2009; Dvorkin et al., 2014). The main nonlinearity in the rock-physics model is generally due to the fluid effect. Ball et al. (2014) show that the nonlinear behavior in Gassmann's equation with respect to water saturation is due to the fluid-mixture model, where the fluid bulk modulus is expressed by the isostress average (Mavko et al., 2009):

$$\frac{1}{K_{\text{fl}}} = \frac{s_{\text{w}}}{K_{\text{w}}} + \frac{1 - s_{\text{w}}}{K_{\text{hc}}}, \tag{10}$$

where K_{w} is the water bulk modulus, K_{hc} is the hydrocarbon bulk modulus, and s_{w} is the water saturation. Additionally, Ball et al. (2014) also point out that the saturated-rock bulk modulus obtained from Gassmann's equation is almost linear with respect to the fluid bulk modulus, as shown in Figure 1b. Furthermore, equation 9 indicates that ρ_{sat} is linear with respect to ρ_{fl}. Therefore, we conclude that even though a linearization of the saturated-rock elastic properties in terms of the fluid saturations is not possible in the presence of multiple fluids, a linearization of the saturated-rock elastic properties in terms of the fluid elastic properties provides accurate results. Finally, the relation between porosity and the saturated-rock density is linear, and the relation between porosity and the saturated-rock elastic properties is almost linear, as shown in Figure 1c.

Therefore, instead of expressing the rock-physics model in terms of the petrophysical properties of interest, such as porosity ϕ, water saturation s_{w}, and clay volume v_{c}, we propose to adopt a model parameterization, including the matrix elastic moduli K_{m}, G_{m} and density ρ_{m}, fluid bulk modulus K_{fl} and density ρ_{fl}, and porosity ϕ. These properties are then the inputs for the rock-physics model for the computation of the saturated-rock bulk modulus K_{sat}, shear modulus G_{sat}, and density ρ_{sat}. In other words, the vector of model parameter $\mathbf{m}$ in equation 1 is equal to $[K_{\text{m}}, G_{\text{m}}, \rho_{\text{m}}, K_{\text{fl}}, \rho_{\text{fl}}, \phi]^T$ and the vector $\mathbf{q}$ is $[K_{\text{sat}}, G_{\text{sat}}, \rho_{\text{sat}}]^T$. The results in Figure 1 show that a linearization of the rock-physics model $\mathbf{g}$ linking $\mathbf{m}$ to $\mathbf{q}$ provide accurate results; however, differently from the seismic linearization model, the rock-physics linearization is not explicitly available and must be numerically computed. Therefore, we derive the linearized expression of the forward model by computing the first-order approximation of Taylor series expansion (Grana, 2016) of the logarithm of the elastic properties:

$$\ln \mathbf{q} \approx \mathbf{g}(\mathbf{m}_0) + \boldsymbol{J}_{\mathbf{m}_0}(\mathbf{m} - \mathbf{m}_0) = \boldsymbol{J}_{\mathbf{m}_0}\mathbf{m} + (\mathbf{g}(\mathbf{m}_0) - \boldsymbol{J}_{\mathbf{m}_0}\mathbf{m}_0), \tag{11}$$

where $\mathbf{m}_0 = [\bar{K}_{\text{m}}, \bar{G}_{\text{m}}, \bar{\rho}_{\text{m}}, \bar{K}_{\text{fl}}, \bar{\rho}_{\text{fl}}, \bar{\phi}]^T$ is assumed to be the mean value of the model parameters. The quantity $\mathbf{g}(\mathbf{m}_0) - \boldsymbol{J}_{\mathbf{m}_0}\mathbf{m}_0$ is a constant value evaluated at $\mathbf{m}_0$, and $\boldsymbol{J}_{\mathbf{m}_0} = \boldsymbol{J}(\mathbf{m})|_{\mathbf{m}=\mathbf{m}_0}$ is the Jacobian of the rock-physics model, which can be written as evaluated at $\mathbf{m}_0$:

$$\boldsymbol{J}(\mathbf{m})|_{\mathbf{m}=\mathbf{m}_0} = \begin{bmatrix} \frac{\partial \ln K_{\text{sat}}}{\partial K_{\text{m}}} & \frac{\partial \ln K_{\text{sat}}}{\partial G_{\text{m}}} & \frac{\partial \ln K_{\text{sat}}}{\partial \rho_{\text{m}}} & \frac{\partial \ln K_{\text{sat}}}{\partial K_{\text{fl}}} & \frac{\partial \ln K_{\text{sat}}}{\partial \rho_{\text{fl}}} & \frac{\partial \ln K_{\text{sat}}}{\partial \phi} \\ \frac{\partial \ln G_{\text{sat}}}{\partial K_{\text{m}}} & \frac{\partial \ln G_{\text{sat}}}{\partial G_{\text{m}}} & \frac{\partial \ln G_{\text{sat}}}{\partial \rho_{\text{m}}} & \frac{\partial \ln G_{\text{sat}}}{\partial K_{\text{fl}}} & \frac{\partial \ln G_{\text{sat}}}{\partial \rho_{\text{fl}}} & \frac{\partial \ln G_{\text{sat}}}{\phi} \\ \frac{\partial \ln \rho_{\text{sat}}}{\partial K_{\text{m}}} & \frac{\ln \rho_{\text{sat}}}{\partial G_{\text{m}}} & \frac{\partial \ln \rho_{\text{sat}}}{\partial \rho_{\text{m}}} & \frac{\partial \ln \rho_{\text{sat}}}{\partial K_{\text{fl}}} & \frac{\partial \ln \rho_{\text{sat}}}{\partial \rho_{\text{fl}}} & \frac{\partial \ln \rho_{\text{sat}}}{\partial \phi} \end{bmatrix}_{|\mathbf{m}=\mathbf{m}_0}. \tag{12}$$

Appendix A shows the expression of the Jacobian. We then combine equations 11 and 12 with equation 4 to obtain

$$\begin{aligned} r_{\text{pp}} = {} & \left(\frac{1}{4} - \frac{1}{3\gamma^2}\right)\sec^2\theta \frac{\partial}{\partial t}(c_{11}K_{\text{m}} + c_{12}G_{\text{m}} + c_{13}\rho_{\text{m}} \\ & + c_{14}K_{\text{fl}} + c_{15}\rho_{\text{fl}} + c_{16}\phi + \text{const}_1) \\ & + \frac{1}{\gamma^2}\left(\frac{\sec^2\theta}{3} - 2\sin^2\theta\right)\frac{\partial}{\partial t}(c_{21}K_{\text{m}} + c_{22}G_{\text{m}} + c_{23}\rho_{\text{m}} \\ & + c_{24}K_{\text{fl}} + c_{25}\rho_{\text{fl}} + c_{26}\phi + \text{const}_2) \\ & + \left(\frac{2 - \sec^2\theta}{4}\right)\frac{\partial}{\partial t}(c_{31}K_{\text{m}} + c_{32}G_{\text{m}} + c_{33}\rho_{\text{m}} \\ & + c_{34}K_{\text{fl}} + c_{35}\rho_{\text{fl}} + c_{36}\phi + \text{const}_3), \end{aligned} \tag{13}$$

where the expression of the coefficients c_{ij} (for $i = 1, \ldots 3$ and $j = 1, \ldots, 6$) is given in Appendix A. By substituting the explicit expressions of the Jacobian in equation 13, we obtain the new formulation

$$\begin{aligned} r_{\text{pp}}(t,\theta) = {} & a_{K_{\text{m}}}\frac{\partial}{\partial t}K_{\text{m}}(t) + a_{G_{\text{m}}}\frac{\partial}{\partial t}G_{\text{m}}(t) + a_{\rho_{\text{m}}}\frac{\partial}{\partial t}\rho_{\text{m}}(t) \\ & + a_{K_{\text{fl}}}\frac{\partial}{\partial t}K_{\text{fl}}(t) + a_{\rho_{\text{fl}}}\frac{\partial}{\partial t}\rho_{\text{fl}}(t) + a_{\phi}\frac{\partial}{\partial t}\phi(t), \end{aligned} \tag{14}$$

where

$$a_{K_{\text{m}}} = c_{11}\left(\frac{1}{4} - \frac{1}{3\gamma^2}\right)\sec^2\theta, \tag{15}$$

$$a_{G_{\text{m}}} = \frac{c_{22}}{\gamma^2}\left(\frac{\sec^2\theta}{3} - 2\sin^2\theta\right), \tag{16}$$

$$a_{\rho_{\text{m}}} = c_{33}\left(\frac{2 - \sec^2\theta}{4}\right), \tag{17}$$

$$a_{K_{\text{fl}}} = c_{14}\left(\frac{1}{4} - \frac{1}{3\gamma^2}\right)\sec^2\theta, \tag{18}$$

$$a_{\rho_{\text{fl}}} = c_{35}\left(\frac{2 - \sec^2\theta}{4}\right), \tag{19}$$

$$\begin{aligned} a_{\phi} = {} & c_{16}\left(\frac{1}{4} - \frac{1}{3\gamma^2}\right)\sec^2\theta + \frac{c_{26}}{\gamma^2}\left(\frac{\sec^2\theta}{3} - 2\sin^2\theta\right) \\ & + c_{36}\left(\frac{2 - \sec^2\theta}{4}\right). \end{aligned} \tag{20}$$

Inversion model

By combining equation 2 with equation 14, we obtain a joint seismic-petrophysics linearized forward model:

$$\mathbf{d} = \mathbf{WADm} + \boldsymbol{\varepsilon} = \mathbf{Gm} + \boldsymbol{\varepsilon}, \tag{21}$$

where the matrix $\mathbf{A}$ contains the coefficients $a_{K_{\text{m}}}$, $a_{G_{\text{m}}}$, $a_{\rho_{\text{m}}}$, $a_{K_{\text{fl}}}$, $a_{\rho_{\text{fl}}}$, and a_{ϕ} (equations 15–20); $\mathbf{D}$ is the first-order difference matrix; and $\mathbf{G}$ is equal to $\mathbf{WAD}$. This formulation is similar to the linearized

AVO formulation proposed in Buland and Omre (2003); however, in our formulation, the model vector $\mathbf{m}$ includes petrophysical parameters (rather than elastic parameters as in Buland and Omre, 2003) and the matrix $\mathbf{A}$ contains the coefficients of the new formulation (equations 13–20) rather than the traditional Aki-Richards coefficients, as in Buland and Omre (2003).

To solve the inverse problem, for the estimation of rock and fluid properties, in this work we propose a Bayesian approach based on Gaussian and linear assumptions (Tarantola, 2005). However, we point out that any linear inverse method could be applied. In the Bayesian approach, the posterior distribution of the model given the data $P(\mathbf{m}|\mathbf{d})$ is proportional to the product of the likelihood function times the prior distribution $P(\mathbf{m}|\mathbf{d}) \propto P(\mathbf{d}|\mathbf{m})P(\mathbf{m})$. We assume that the prior distribution of the model $\mathbf{m} = [K_m, G_m, \rho_m, K_{fl}, \rho_{fl}, \phi]^T$ is distributed as a Gaussian distribution $\mathbf{m} \sim N(\mathbf{m}; \boldsymbol{\mu}_\mathbf{m}, \boldsymbol{\Sigma}_\mathbf{m})$ and that the error term $\boldsymbol{\varepsilon} \sim N(\boldsymbol{\varepsilon}; 0, \boldsymbol{\Sigma}_\varepsilon)$ is also Gaussian distribution with zero mean and covariance $\boldsymbol{\Sigma}_\varepsilon$. The prior covariance matrix $\boldsymbol{\Sigma}_\mathbf{m}$ can also include a spatial correlation model by combining the time-invariant covariance matrix of the model properties with a vertical correlation function, as in Buland and Omre (2003). Then, the posterior distribution of model parameters $\mathbf{m}|\mathbf{d} \sim N(\mathbf{m}; \boldsymbol{\mu}_{\mathbf{m}|\mathbf{d}}, \boldsymbol{\Sigma}_{\mathbf{m}|\mathbf{d}})$ is also a Gaussian distribution and the posterior mean $\boldsymbol{\mu}_{\mathbf{m}|\mathbf{d}}$ and covariance matrix $\boldsymbol{\Sigma}_{\mathbf{m}|\mathbf{d}}$ can be written in the following analytical form (Buland and Omre, 2003; Tarantola, 2005):

$$\boldsymbol{\mu}_{\mathbf{m}|\mathbf{d}} = \boldsymbol{\mu}_\mathbf{m} + \boldsymbol{\Sigma}_\mathbf{m}\mathbf{G}^T(\mathbf{G}\boldsymbol{\Sigma}_\mathbf{m}\mathbf{G}^T + \boldsymbol{\Sigma}_\varepsilon)^{-1}(\mathbf{d} - \mathbf{G}\boldsymbol{\mu}_\mathbf{m}), \quad (22)$$

$$\boldsymbol{\Sigma}_{\mathbf{m}|\mathbf{d}} = \boldsymbol{\Sigma}_\mathbf{m} - \boldsymbol{\Sigma}_\mathbf{m}\mathbf{G}^T(\mathbf{G}\boldsymbol{\Sigma}_\mathbf{m}\mathbf{G}^T + \boldsymbol{\Sigma}_\varepsilon)^{-1}\mathbf{G}\boldsymbol{\Sigma}_\mathbf{m}. \quad (23)$$

Our approach allows predicting the most likely values and the associated uncertainty (equations 22 and 23, respectively) of the reservoir model parameters $\mathbf{m}$ (i.e., the matrix elastic moduli and density, the fluid bulk modulus and density, and porosity, according to our parameterization).

The forward model in matrix $\mathbf{G}$ depends on the value $\mathbf{m}_0$ used in the linearization using Taylor's series truncation. The formulation in equations 13–20 assumes that $\mathbf{m}_0 = [\bar{K}_m, \bar{G}_m, \bar{\rho}_m, \bar{K}_{fl}, \bar{\rho}_{fl}, \bar{\phi}]^T$ is constant and is equal to the mean value of the model parameters because the value of the parameters is unknown priori. However, if the value is far from the actual solution, the linearization might be inaccurate for models with strong nonlinearities. To mitigate the problem, we propose an iterative approach in which we assume $\mathbf{m}_0 = [\bar{K}_m, \bar{G}_m, \bar{\rho}_m, \bar{K}_{fl}, \bar{\rho}_{fl}, \bar{\phi}]^T$, compute the solution of the inversion problem, update the $\mathbf{m}_0$ value as $\mathbf{m}_0 = \boldsymbol{\mu}_{\mathbf{m}|\mathbf{d}}$, and iterate until convergence. Despite the lack of a convergence proof, there is numerical evidence that the method should converge, at least for monotonic functions. The iterative algorithm is as follows (Algorithm 1):

Algorithm 1. Iterative Bayesian linearized inversion.

1 Initialize $\mathbf{m}_0 = [\bar{K}_m, \bar{G}_m, \bar{\rho}_m, \bar{K}_{fl}, \bar{\rho}_{fl}, \bar{\phi}]^T$
2 Compute posterior mean $\boldsymbol{\mu}_{\mathbf{m}|\mathbf{d}}$ and covariance $\boldsymbol{\Sigma}_{\mathbf{m}|\mathbf{d}}$
3 Select a tolerance T
4 **While** $\|\mathbf{d} - \mathbf{G}(\boldsymbol{\mu}_{\mathbf{m}|\mathbf{d}})\| < T$ do
5 Set $\mathbf{m}_0 = \boldsymbol{\mu}_{\mathbf{m}|\mathbf{d}}$
6 Update $\mathbf{G}$
7 Compute posterior mean $\boldsymbol{\mu}_{\mathbf{m}|\mathbf{d}}$ and covariance $\boldsymbol{\Sigma}_{\mathbf{m}|\mathbf{d}}$
8 **end**

If the rock and fluid parameters are known, petrophysical properties such as mineral volumes (for example, clay content) and fluid saturations (for example, water saturation) can be computed by solving a nonlinear inversion based on Voigt-Reuss-Hill averages and mass balance equations (Mavko et al., 2009). The estimation of the posterior distributions of rock and fluid fractions can be analytically computed if the inverse function is defined. If we assume a mixture of two minerals (for example, clay and quartz) and two fluids (for example, water and hydrocarbon), we can use the following forward model:

$$K_m = \frac{1}{2}\left(v_c K_c + (1 - v_c)K_q + \frac{1}{v_c/K_c + (1 - v_c)/K_q}\right), \quad (24)$$

$$G_m = \frac{1}{2}\left(v_c G_c + (1 - v_c)G_q + \frac{1}{v_c/G_c + (1 - v_c)/G_q}\right), \quad (25)$$

$$\rho_m = v_c\rho_c + (1 - v_c)\rho_q, \quad (26)$$

$$K_{fl} = \frac{1}{s_w/K_w + (1 - s_w)/K_{hc}}, \quad (27)$$

$$\rho_{fl} = s_w\rho_c + (1 - s_w)\rho_{hc}, \quad (28)$$

where K_c and K_q are the bulk moduli of clay and quartz, respectively, G_c and G_q are their shear moduli, and ρ_c and ρ_q are their densities; and K_w and K_{hc} are the bulk moduli of water and hydrocarbon, and ρ_w and ρ_{hc} are their densities. All these parameters are assumed to be constant and known (for example, from the literature or from laboratory measurements). The clay volume can be then expressed as a function of three random variables, namely, K_m, G_m, and ρ_m; and the water saturation can be expressed as a function of two random variables, namely, K_{fl} and ρ_{fl}.

If the distribution of the rock and fluid properties is known at a given depth (from the Bayesian linearized petrophysical inversion,

Table 1. Model parameters for three different geologic models (two-layer, single-interface model). For each model, the top row shows the values of the top layer, and the bottom row shows the values of the bottom layer.

	K_m (GPa)	G_m (GPa)	ρ_m (g/cm^3)	K_{fl} (GPa)	ρ_{fl} (g/cm^3)	ϕ
Model 1	36.00	45.00	2.65	2.25	1.03	0.25
	29.00	36.00	2.57	2.25	1.03	0.25
Model 2	36.00	45.00	2.65	0.63	0.64	0.25
	36.00	45.00	2.65	2.25	1.03	0.25
Model 3	36.00	45.00	2.65	2.25	1.03	0.25
	36.00	45.00	2.65	2.25	1.03	0.15

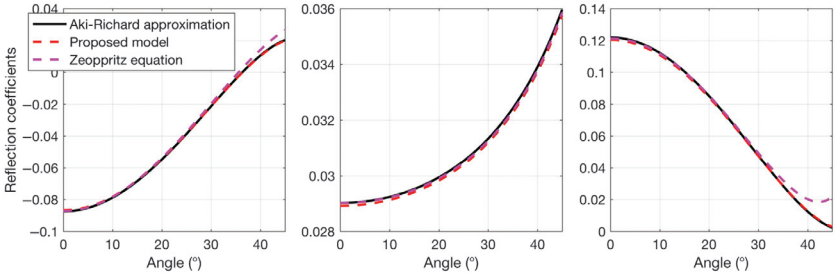

Figure 2. Comparison between reflection coefficients derived from the traditional Aki-Richards approximation (solid black lines), full Zoeppritz equations (dotted magenta lines), and the new proposed formulation (dotted red lines) as a function of the incident angle for a two-layer model. (a) Model 1 with different mineral compositions in the top and bottom layers, (b) model 2 with different fluid saturations in top and bottom layers, and (c) model 3 with different porosity values in top and bottom layers.

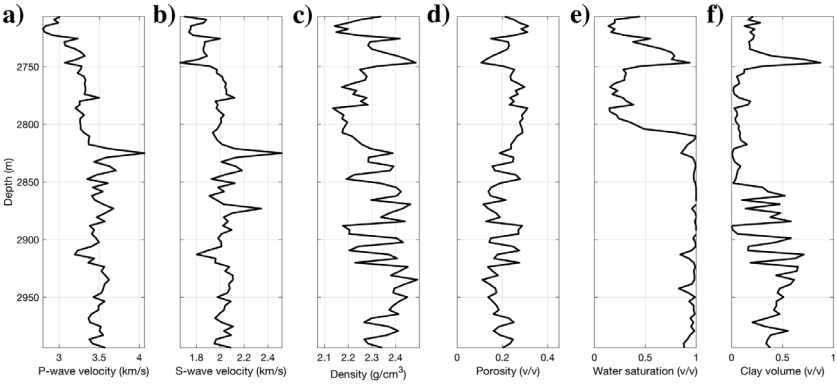

Figure 3. Well logs and interpreted curves of the reference well. (a) P-wave velocity, (b) S-wave velocity, (c) density, (d) porosity, (e) water saturation, and (f) clay volume.

equations 22 and 23), then the posterior distributions of clay volume and water saturation, $f_{v_c}(v_c)$ and $f_{s_w}(s_w)$, respectively, can be computed as a function of random variables (Papoulis, 1984):

$$f_{v_c}(v_c) = \frac{d}{dv_c} F_{v_c}(v_c) = \frac{d}{dv_c} \int_{d_3}^{\rho_q} \int_{d_2}^{G_q} \int_{d_1}^{K_q} f_{K_m,G_m,\rho_m}(K_m, G_m, \rho_m) \times dK_m dG_m d\rho_m, \quad (29)$$

$$f_{s_w}(s_w) = \frac{d}{ds_w} F_{s_w}(s_w) = \frac{d}{ds_w} \int_{\rho_{hc}}^{c_2} \int_{K_{hc}}^{c_1} f_{K_{fl},\rho_{fl}}(K_{fl}, \rho_{fl}) dK_{fl} d\rho_{fl}, \quad (30)$$

where $F_{v_c}(v_c)$ and $F_{s_w}(s_w)$ are the cumulative density functions (cdf) of the clay volume and water saturation; the expressions of d_1, d_2, d_3, c_1, and c_2 are computed from equations 24–28, respectively (see Appendix B), and $f_{K_m,G_m,\rho_m}(K_m,G_m,\rho_m) = N(\boldsymbol{\mu}_{K_m,G_m,\rho_m|\mathbf{d}}, \boldsymbol{\Sigma}_{K_m,G_m,\rho_m|\mathbf{d}})$; and $f_{K_{fl},\rho_{fl}}(K_{fl},\rho_{fl}) = N(\boldsymbol{\mu}_{K_{fl},\rho_{fl}|\mathbf{d}}, \boldsymbol{\Sigma}_{K_{fl},\rho_{fl}|\mathbf{d}})$ are the marginal probability density functions of the rock and fluid parameters obtained from equations 22 and 23. The derivation of the integration domain is shown in Appendix B. Alternatively, the posterior distributions of the rock and fluid fractions could be evaluated by applying the method proposed by Buland et al. (2008).

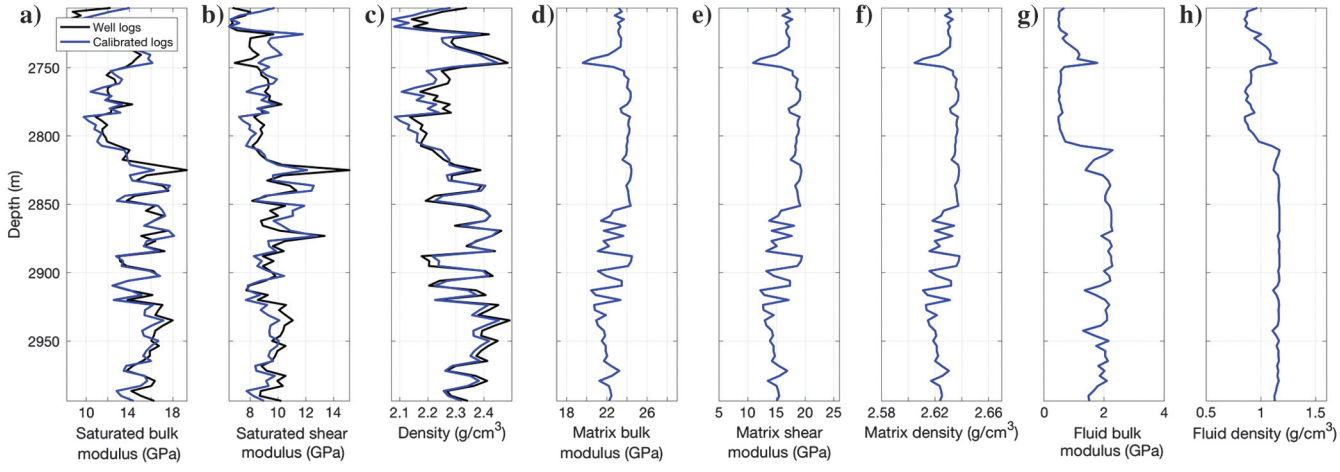

Figure 4. Rock and fluid properties computed from well logs and predicted using the exact rock-physics model. (a) saturated-rock bulk modulus, (b) saturated-rock shear modulus, (c) saturated-rock density, (d) matrix bulk modulus, (e) matrix shear modulus, (f) matrix density, (g) fluid bulk modulus, and (h) fluid density. The black lines are calculated from the well logs; the blue lines are calculated using the rock-physics model.

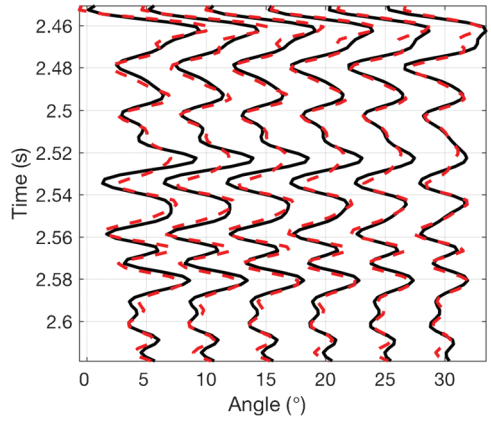

Figure 5. Comparison between the synthetic seismic data computed by the Aki-Richards approximation (equation 3, solid black lines) and the new formulation (equation 14, dotted red lines).

APPLICATIONS

Illustrative example

We first created three simple two-layer geologic models (Table 1) to verify the accuracy of the linearized model compared with the actual rock-physics model. In particular, we compare the reflection coefficients derived through the Aki-Richards approximation (where the elastic properties of the two layers are computed using the full rock-physics model) and those computed through the new proposed approximation, as a function of the incident angle. In the three examples, we assumed that the contrast is caused by changes in the mineralogy, the fluid content, and the pore-space volume, respectively. In the first model, the top layer is clean sand with 100% quartz and the bottom layer is sand with 40% clay (Table 1). We assume that both layers are fully saturated by water and the porosity is equal to 0.25 in both layers. In the second model, we assume a high-porosity sandstone in both layers; the top layer is

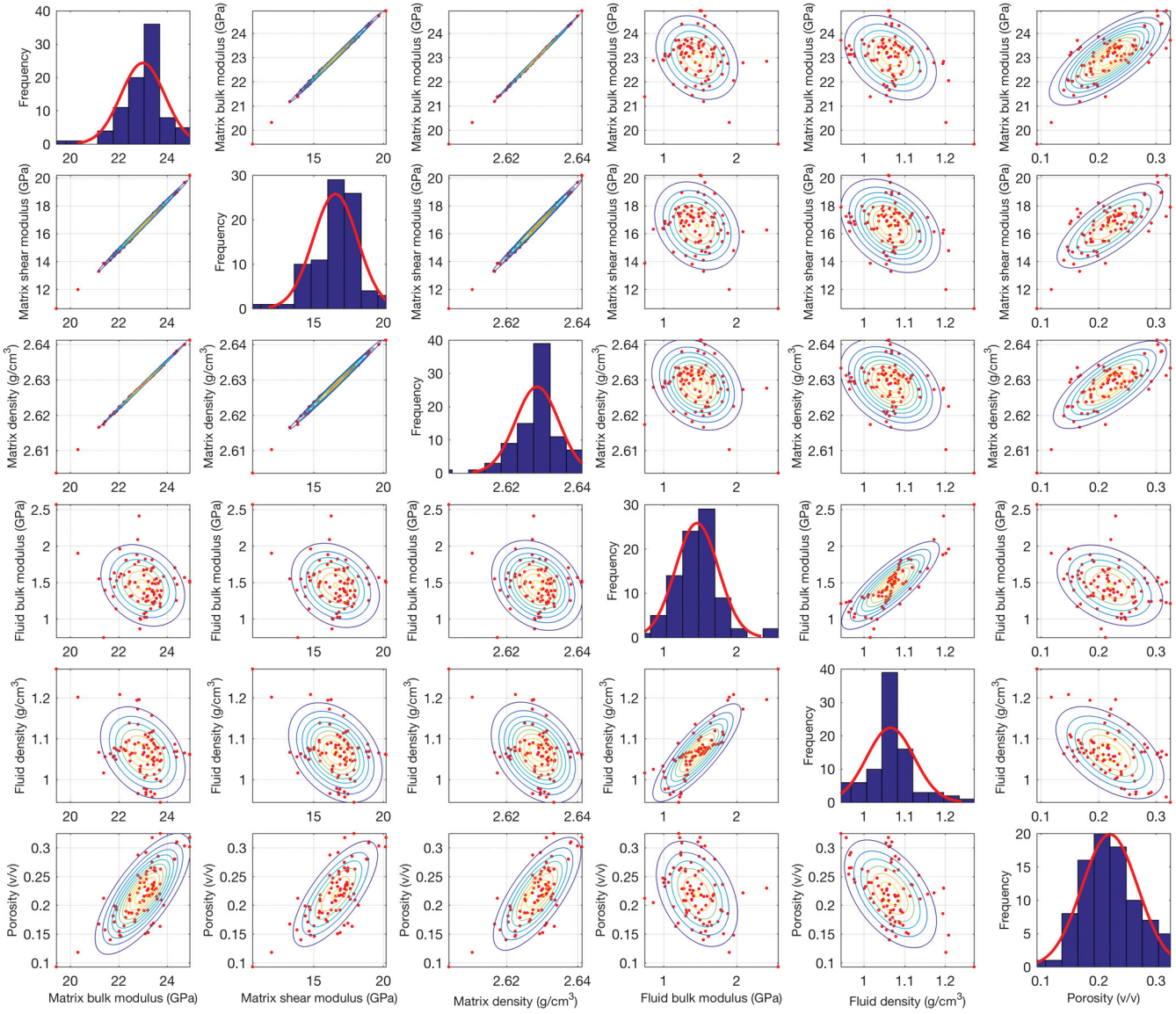

Figure 6. Histograms and bivariate distributions of detrended well-log data and corresponding marginal distributions. The univariate marginal distributions are normalized to allow the comparison with the corresponding histograms in the frequency domain.

partially saturated by gas, and the bottom layer is fully saturated by water (Table 1). In the third model, we assume a water-saturated sandstone in both layers; the porosity of the top layer is 0.25, and the porosity of the bottom layer is 0.15 (Table 1). The computed reflection coefficients for these three models are shown in Figure 2.

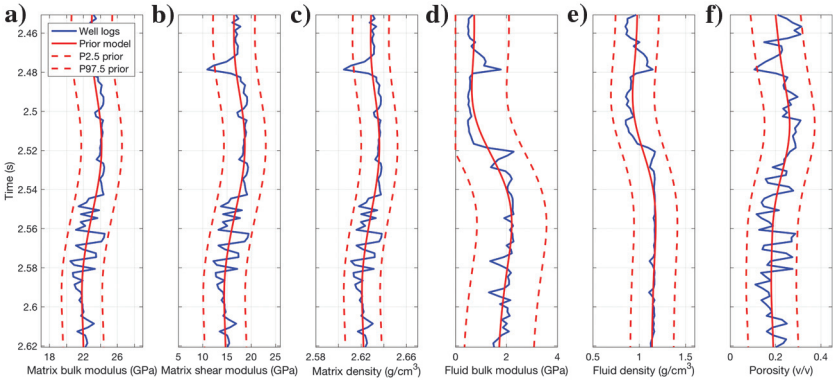

Figure 7. Prior distribution of the model parameters: (a) matrix bulk modulus, (b) matrix shear modulus, (c) matrix density, (d) fluid bulk modulus, (e) fluid density, and (f) porosity. The blue lines represent the reference values; the red lines represent the 95% confidence interval of the prior distribution (the solid lines represent the mean, and the dashed lines represent the percentiles).

Table 2. Correlation matrix of the prior model.

	K_m	G_m	ρ_m	K_{fl}	ρ_{fl}	ϕ
K_m	1	0.9	0.9	−0.4	−0.4	0.7
G_m	0.9	1	0.9	−0.4	−0.4	0.7
ρ_m	0.9	0.9	1	−0.4	−0.4	0.7
K_{fl}	−0.4	−0.4	−0.4	1	0.9	−0.6
ρ_{fl}	−0.4	−0.4	−0.4	0.9	1	−0.6
ϕ	0.7	0.7	0.7	−0.6	−0.6	1

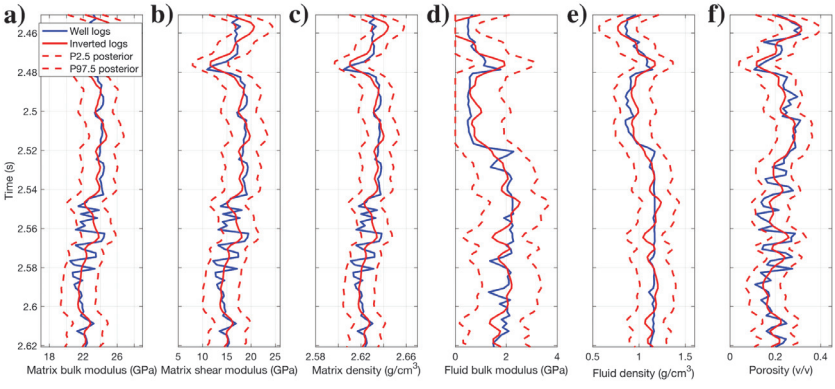

Figure 8. Inversion of synthetic seismic data (Figure 5). Posterior probability distribution of (a) matrix bulk modulus, (b) matrix shear modulus, (c) matrix density, (d) fluid bulk modulus, (e) fluid density, and (f) porosity. The legend and colors are as in Figure 7.

The AVO curves derived from the new approximation (equation 14) provide a good approximation of those obtained from the Aki-Richards approximation (equation 3). For completeness of the information, we also computed the results to the reflection coefficients obtained from the full Zoeppritz equations (Figure 2); if the Aki-Richards approximation is not valid, then our linearized petrophysical AVO approximation also fails.

Synthetic and real-data example

In the following subsections, we apply the inversion method to the Norne field data set. The field includes two compartments: the Norne main structure consisting of the Norne C, D, and E segments, and the northeast segment consisting of the Norne G segment. In this study, we focus on segment E, situated at the northernmost part of the field, and it includes an oil reservoir in the IIe and Tofte Formations, in the Lower and Middle Jurassic age (Steffensen and Karstad, 1995; Osdal et al., 2006; Suman and Mukerji, 2013). The available data include a set of well logs from a reference well and a preprocessed partial-stacked seismic survey with three partial angle stacks acquired in 2001. Well-log data are shown in Figure 3 and include the P-wave velocity, S-wave velocity, density, porosity, water saturation, and clay volume.

We first calibrate the rock-physics model at the well location. The solid phase is made of a mixture of clay minerals ($K_c = 19$ GPa, $G_c = 10$ GPa, $\rho_c = 2.59$ g/cm^3) and a mixture of quartz and feldspar ($K_q = 25$ GPa, $G_q = 20$ GPa, $\rho_q = 2.64$ g/cm^3); the matrix bulk and shear moduli are computed using the Voigt-Reuss-Hill average. The critical porosity is equal to 0.49 according to an average value estimated in the interval of interest. To calculate the fluid bulk modulus, we use the Reuss average (equation 10). The rock-physics model includes Nur's critical porosity model, Gassmann's equation, and the density equation, and it is assumed to be the same in the different facies. Because of the low effective porosity of clay, the rock-physics model in the intervals with high clay volume reduces to the elastic and density averages for the shale (as in Grana and Della Rossa, 2010). Figure 4 shows the comparison between the rock-physics model predictions and the actual data computed from the sonic log (Figure 3).

First, we apply the inversion method to a synthetic seismic data set computed using the actual well logs and assuming a signal-to-noise ratio equal to 2.5; then, we apply the inversion method to the observed seismic trace collocated at the well location and to a 2D seismic section passing through the well location. Initially, we generated a set of synthetic seismograms, including six partial angle stacks corresponding to the angles 5°, 10°, 15°, 20°, 25°, and 30°, with a sampling rate of 2 ms, using a Ricker wavelet with zero-phase and dominant frequency of 40 Hz for all the angle stacks. In Figure 5, we show the synthetic data computed using the

convolution model with reflectivity coefficients computed using the Aki-Richards approximation (equation 3, the solid black lines) and the new approach (equation 14, the dotted red lines).

The inversion workflow is then applied to the synthetic seismic data generated by the Aki-Richards approximation. The goal is to derive the posterior probability distribution of the six reservoir properties of interest (matrix bulk modulus, matrix shear modulus, matrix density, fluid bulk modulus, fluid shear modulus, and porosity) given the seismic data. Overall, the data are not Gaussian because of the presence of depth trends; however, the distribution of the model properties can be locally approximated with a Gaussian distribution with locally variable mean equal to the low-frequency trend. In Figure 6, we show the univariate and bivariate marginal distributions of the model parameters, where we detrended the data (i.e., we subtracted the low-frequency trend and added a constant mean value).

For the prior model, we then assume a Gaussian distribution with a variable mean obtained from a low-frequency model obtained by filtering the actual well-log data. The prior means and the 95% confidence intervals are shown in Figure 7. The prior variances are assumed to be equal to the variances of the properties computed from the well logs. The prior correlation matrix (Table 2) is estimated from well-log data, and it shows a high correlation between some of the model properties (for example, the matrix bulk modulus and matrix shear modulus).

By applying equations 22 and 23, we compute the mean and the covariance matrix of the posterior distribution of the model parameters. The inverted results are shown in Figure 8. Overall, the inverted results are satisfactory because the reference property values (the blue lines) fall inside the high-probability region and the predicted property values (the solid red lines) match the reference model, as shown by the coverage ratios and correlations, respectively (Table 3). The coverage ratio is defined as the percentage of reference values falling inside the 95% confidence interval (the dashed red lines), and it measures the quality of the uncertainty quantification. The correlation between predicted and reference properties quantifies the accuracy of the inverted most likely model. In general, the correlation values are relatively low due to the limited resolution of the inverted model.

Then, we apply inverse approach to the real seismic data set to estimate the posterior distribution of the model parameters. Figure 9 shows a 2D seismic line passing through the well. The near angle corresponds to 10°, the mid angle to 23°, and the far angle to 35°. The sampling rate of the seismic data is 4 ms. The wavelets for each angle stacks are extracted from the seismic data and are zero phase with dominant frequencies equal to 24, 22, and 21 Hz, respectively. The signal-to-noise ratio of the data set is approximately 2.0. We use the same prior model as in the synthetic example. First, we apply the inversion workflow at the well location. The inverted results are shown in Figure 10. The accuracy and precision of the inversion are quantified in Table 3.

Water saturation and clay volume can be estimated from the predicted properties by solving

Table 3. Coverage ratio and correlations of the model properties for the synthetic and real case application at the well location.

	Correlation (synthetic)	Coverage ratio (synthetic)	Correlation (real)	Coverage ratio (real)
K_m	0.74	0.977	0.65	0.953
G_m	0.75	0.977	0.66	0.965
ρ_m	0.73	0.977	0.64	0.942
K_{fl}	0.86	1	0.91	1
ρ_{fl}	0.90	1	0.91	1
ϕ	0.82	0.977	0.67	0.977

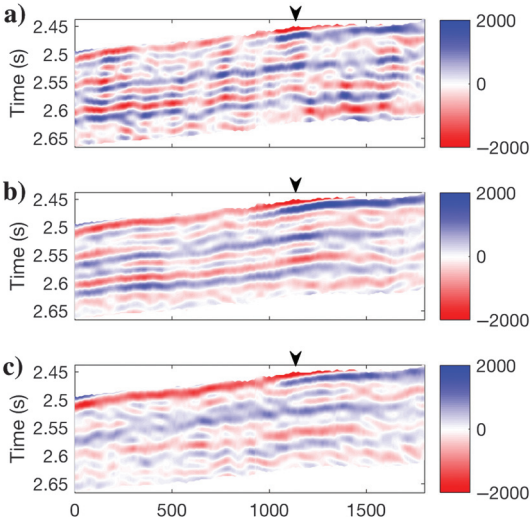

Figure 9. Two-dimensional seismic sections passing through the well location (black triangle): (a) angle stack 10°, (b) angle stack 23°, and (c) angle stack 35°.

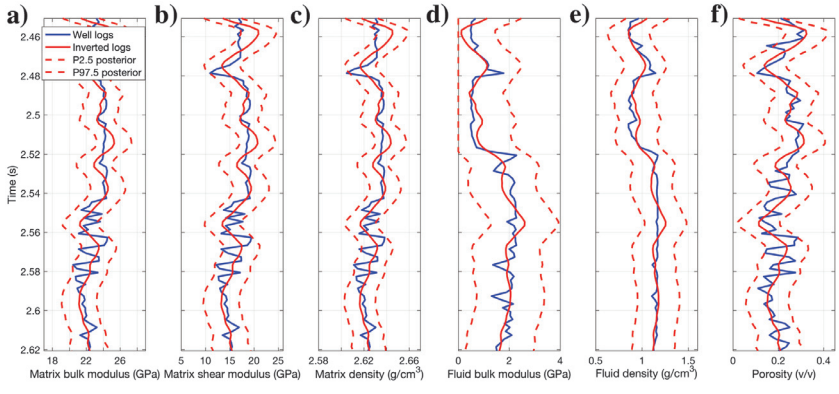

Figure 10. Inversion of real seismic data at the well location. Posterior probability distribution of (a) matrix bulk modulus, (b) matrix shear modulus, (c) matrix density, (d) fluid bulk modulus, (e) fluid density, and (f) porosity. The legend and colors are as in Figure 7.

a nonlinear inversion based on Voigt-Reuss-Hill averages. We analytically compute the cdf of water saturation and clay volume, and we compute their posterior distribution by evaluating the numerical derivatives of the cdfs (equations 29 and 30). The inverted results are shown in Figure 11 (the plot includes porosity that is directly obtained from the Bayesian linear inversion). The marginal posterior distributions of water saturation and clay volume are not Gaussian anymore but are skewed toward the boundaries of the property ranges.

Finally, we apply inverse approach to a 2D seismic section with three angle stacks. The approach is applied trace by trace. The prior model is built by interpolating the prior model at the well location along the seismic horizon of the 2D seismic section, assuming a constant covariance matrix. The inverted results of the matrix bulk modulus, matrix shear modulus, matrix density, fluid bulk modulus, fluid density, and porosity obtained using a Bayesian Gaussian linearized inversion are shown in Figure 12, and the inverted results of porosity, water saturation, and clay volume obtained using nonlinear relations are shown in Figure 13. Well-log data are superimposed to the 2D sections for comparison purposes and show a good match.

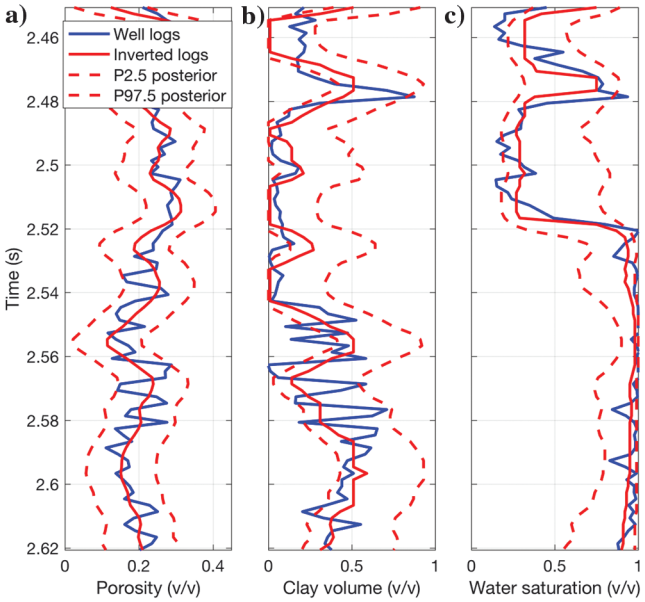

Figure 11. Inverted petrophysical parameters at the well location. (a) Porosity, (b) clay volume, and (c) water saturation. The legend and colors are as in Figure 7.

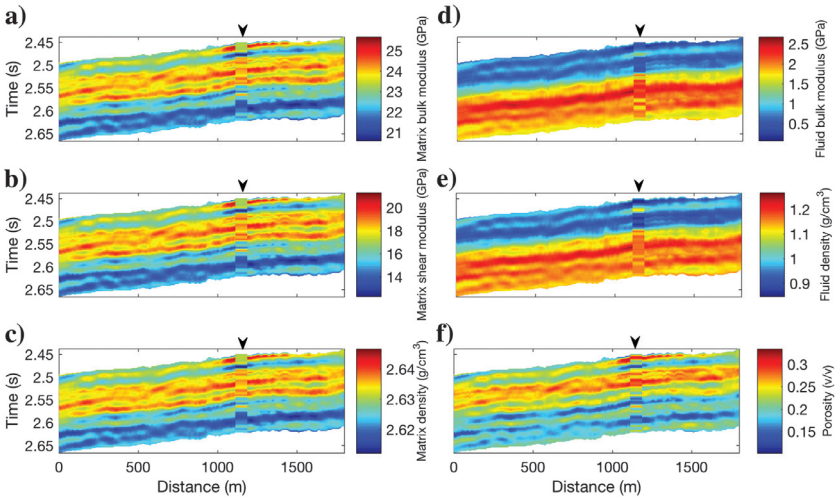

Figure 12. Two-dimensional sections of inverted model parameters: (a) matrix bulk modulus, (b) matrix shear modulus, (c) matrix density, (d) fluid bulk modulus, (e) fluid density, and (f) porosity. The black triangle indicates the well location.

DISCUSSION

Our linearized petrophysical AVO approximation is presented for a rock-physics model that combines Gassmann's equation and Nur's critical porosity model, but it could be extended to other models, such as inclusion and granular media models because the linearization is computed using Taylor series expansions (Grana, 2016). However, such an extension might require the numerical evaluation of the first-order partial derivatives of the Jacobian of the rock-physics model due to the complexity of the model equations. In some applications, the numerical expression of the Jacobian might also be more robust than the analytical approximation. We point out that linearized approximations might fail for some rock-physics equations that are nonlinear in some of the model parameters, such as the soft sand model with respect to porosity or the homogeneous fluid mixture with respect to the fluid saturations.

The linearized petrophysical AVO approximation can be used in a single-loop inversion workflow to predict the reservoir properties of interest. In our approach, we adopt a Bayesian Gaussian-linear inversion method (Buland and Omre, 2003) to estimate the posterior distribution of the model parameters; however, any other linear inverse method could be used. The advantage of our formulation is that the linearization of the forward model allows estimating the solution of the inverse problem using analytical forms resulting in low computational effort. The drawback of our method is that the forward model is linear in a parameterization that includes elastic moduli and density of the solid and fluid phases rather than mineral volumes and fluid saturations. However, the volumetric fractions of interest can be estimated using a nonlinear inversion. A limitation of our approach for practical applications is due to the number of model variables, which is generally larger than the number of measured data, i.e., the number of partial angle stacks. If the number of partial angle stacks is less than the number of model variables, the problem is underdetermined. Such a limitation can be mitigated by imposing a strong correlation between some of the model variables in the prior distribution, for example, assuming that the bulk and shear modulus of the solid have correlation close to one. Such an assumption, however, should be validated using laboratory measurements or well-log data.

In our approach, we adopted the same rock-physics model; however, different models could be used in different lithologies if a preliminary facies classification is available (as in Ulvmoen and Omre, 2010) or in a joint facies/rock-physics inversion workflow (as in Rimstad and

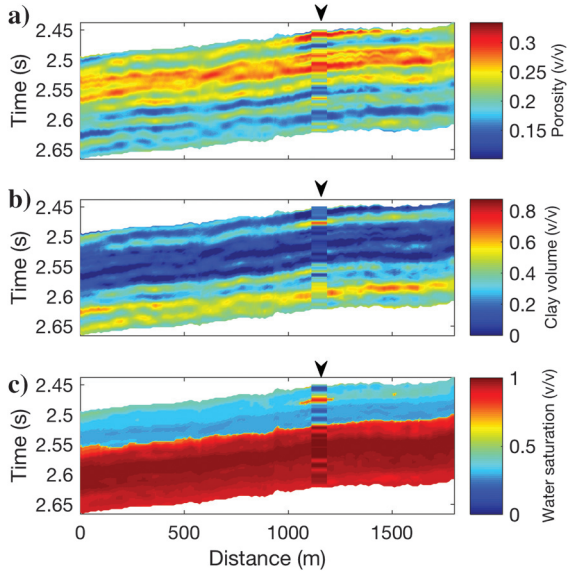

Figure 13. Two-dimensional sections of inverted petrophysical parameters: (a) porosity, (b) clay volume, and (c) water saturation. The black triangle indicates the well location.

Omre, 2010; Grana et al., 2017). Our approach is applied trace by trace. The inversion method includes a vertical correlation function, estimated from the reference well logs, to account for the spatial continuity of the model in the vertical component. The spatial continuity in the seismic data guarantees a lateral continuity in the inverted model; however, a spatial correlation function in the lateral direction could also be included (as in Ulvmoen and Omre, 2010).

CONCLUSION

We presented a new formulation of a linearized seismic-petrophysics forward model based on the combination of an AVO approximation with a linearized rock-physics model, achieved by applying a first-order truncation of the Taylor's series expansion. In our formulation, the rock-physics model consists of Nur's critical porosity and Gassmann's equations. The parameterization chosen for the model linearization includes porosity as well as the elastic moduli and density of the solid and fluid phases because our formulation is almost linear in these parameters. In our application, the approximated model fits the well-log data and the linearized approximation provides an accurate forward model. The linearization of the model allows using linear inverse theory and obtaining the solution of the reservoir characterization inverse problem in a single-loop inversion with a limited computational effort. In our work, we combine the new formulation with Bayesian Gaussian-linear inverse theory to predict the distribution of the reservoir properties of interest. The application of the linearized petrophysical AVO approximation in the context of geophysical inverse modeling to synthetic and real data set provided satisfactory results.

ACKNOWLEDGMENTS

The authors would like to thank Statoil (operator of the Norne field) and its license partners ENI and Petoro for the release of the Norne data and the Center for Integrated Operations at NTNU for cooperation and coordination of the Norne Cases. The views expressed in this paper are the views of the authors and do not necessarily reflect the views of Statoil and the Norne license partners. Authors also acknowledge the School of Energy Resources and the Department of Geology and Geophysics of the University of Wyoming for the support.

APPENDIX A

PARTIAL DERIVATIVES OF LINEARIZED FORWARD MODEL

First, we show the computation of the elements of the Jacobian matrix in equation 12. The partial derivatives of the log-transformed saturated-rock bulk modulus (K_{sat}) with respect to the model parameters $(K_{\text{m}}, G_{\text{m}}, \rho_{\text{m}}, K_{\text{fl}}, \rho_{\text{fl}}, \phi)$ are

$$c_{11} = \frac{\partial \ln K_{\text{sat}}}{\partial K_{\text{m}}}\Big|_{\mathbf{m}=\mathbf{m}_0} = \frac{\bar{K}_{\text{fl}}^2(1-\phi_0)(1-\phi_0+\bar{\phi}) + 2\bar{K}_{\text{m}}\bar{K}_{\text{fl}}(1-\phi_0)(\phi_0-\bar{\phi}) + \bar{K}_{\text{m}}^2\phi_0(\phi_0-\bar{\phi})}{[\bar{K}_{\text{m}}\bar{K}_{\text{fl}}(1-\phi_0+\bar{\phi}) + \bar{K}_{\text{m}}^2(\phi_0-\bar{\phi})][\bar{K}_{\text{fl}}(1-\phi_0) + \bar{K}_{\text{m}}\phi_0]} \tag{A-1}$$

$$c_{12} = \frac{\partial \ln K_{\text{sat}}}{\partial G_{\text{m}}}\Big|_{\mathbf{m}=\mathbf{m}_0} = 0, \tag{A-2}$$

$$c_{13} = \frac{\partial \ln K_{\text{sat}}}{\partial \rho_{\text{m}}}\Big|_{\mathbf{m}=\mathbf{m}_0} = 0, \tag{A-3}$$

$$c_{14} = \frac{\partial \ln K_{\text{sat}}}{\partial K_{\text{fl}}}\Big|_{\mathbf{m}=\mathbf{m}_0} = \frac{\bar{\phi}\bar{K}_{\text{m}}}{[\bar{K}_{\text{fl}}(1-\phi_0+\bar{\phi}) + \bar{K}_{\text{m}}(\phi_0-\bar{\phi})][\bar{K}_{\text{fl}}(1-\phi_0) + \bar{K}_{\text{m}}\phi_0]}, \tag{A-4}$$

$$c_{15} = \frac{\partial \ln K_{\text{sat}}}{\partial \rho_{\text{fl}}}\Big|_{\mathbf{m}=\mathbf{m}_0} = 0, \tag{A-5}$$

$$c_{16} = \frac{\partial \ln K_{\text{sat}}}{\partial \phi}\Big|_{\mathbf{m}=\mathbf{m}_0} = \frac{\bar{K}_{\text{fl}} - \bar{K}_{\text{m}}}{\bar{K}_{\text{fl}}(1-\phi_0+\bar{\phi}) + \bar{K}_{\text{m}}(\phi_0-\bar{\phi})}. \tag{A-6}$$

The partial derivatives of the log-transformed saturated-rock shear modulus (G_{sat}) with respect to the model parameters $(K_{\text{m}}, G_{\text{m}}, \rho_{\text{m}}, K_{\text{fl}}, \rho_{\text{fl}}, \phi)$ are

$$c_{21} = \frac{\partial \ln G_{\text{sat}}}{\partial K_{\text{m}}}\Big|_{\mathbf{m}=\mathbf{m}_0} = 0, \tag{A-7}$$

$$c_{22} = \frac{\partial \ln G_{\text{sat}}}{\partial G_{\text{m}}}_{|_{\mathbf{m}=\mathbf{m}_0}} = \frac{1}{\bar{G}_{\text{m}}}, \tag{A-8}$$

$$c_{23} = \frac{\partial \ln G_{\text{sat}}}{\partial \rho_{\text{m}}}_{|_{\mathbf{m}=\mathbf{m}_0}} = 0, \tag{A-9}$$

$$c_{24} = \frac{\partial \ln G_{\text{sat}}}{\partial K_{\text{fl}}}_{|_{\mathbf{m}=\mathbf{m}_0}} = 0, \tag{A-10}$$

$$c_{25} = \frac{\partial \ln G_{\text{sat}}}{\partial \rho_{\text{fl}}}_{|_{\mathbf{m}=\mathbf{m}_0}} = 0, \tag{A-11}$$

$$c_{26} = \frac{\partial \ln G_{\text{sat}}}{\partial \phi}_{|_{\mathbf{m}=\mathbf{m}_0}} = \frac{1}{\bar{\phi} - \phi_0}. \tag{A-12}$$

The partial derivatives of the log-transformed saturated-rock density (ρ_{sat}) with respect to the model parameters ($K_{\text{m}}, G_{\text{m}}, \rho_{\text{m}}, K_{\text{fl}}, \rho_{\text{fl}}, \phi$) are

$$c_{31} = \frac{\partial \ln \rho_{\text{sat}}}{\partial K_{\text{m}}}_{|_{\mathbf{m}=\mathbf{m}_0}} = 0, \tag{A-13}$$

$$c_{32} = \frac{\partial \ln \rho_{\text{sat}}}{\partial G_{\text{m}}}_{|_{\mathbf{m}=\mathbf{m}_0}} = 0, \tag{A-14}$$

$$c_{33} = \frac{\partial \ln \rho_{\text{sat}}}{\partial \rho_{\text{m}}}_{|_{\mathbf{m}=\mathbf{m}_0}} = \frac{1-\bar{\phi}}{\bar{\rho}_{\text{m}}(1-\bar{\phi}) + \bar{\rho}_{\text{fl}}\bar{\phi}}, \tag{A-15}$$

$$c_{34} = \frac{\partial \ln \rho_{\text{sat}}}{\partial K_{\text{fl}}}_{|_{\mathbf{m}=\mathbf{m}_0}} = 0, \tag{A-16}$$

$$c_{35} = \frac{\partial \ln \rho_{\text{sat}}}{\partial \rho_{\text{fl}}}_{|_{\mathbf{m}=\mathbf{m}_0}} = \frac{\bar{\phi}}{\bar{\rho}_{\text{m}}(1-\bar{\phi}) + \bar{\rho}_{\text{fl}}\bar{\phi}}, \tag{A-17}$$

$$c_{36} = \frac{\partial \ln \rho_{\text{sat}}}{\partial \phi}_{|_{\mathbf{m}=\mathbf{m}_0}} = \frac{\bar{\rho}_{\text{fl}} - \bar{\rho}_{\text{m}}}{\bar{\rho}_{\text{m}}(1-\bar{\phi}) + \bar{\rho}_{\text{fl}}\bar{\phi}}. \tag{A-18}$$

APPENDIX B

FUNCTION OF MULTIPLE RANDOM VARIABLES

If a random variable z is a function of two (or more) random variables, $z = g(x, y)$, then its cdf $F_z(z)$ can be computed as

$$F_z(z) = \int_{D_z(x,y)} f_{x,y}(x, y)dxdy, \tag{B-1}$$

where $f_{x,y}(x, y)$ is the probability density function of the input variables and the integration domain $D_z(x, y)$ is defined as the region where $g(x, y) \le z$.

In our approach (two minerals and two fluid components), the random variable z can be the clay volume or the water saturation; the function g is the inverse function of equations 24–28; the input variables are the elastic moduli and densities of solid and fluid; and the input pdf is the probability distribution obtained from the Bayesian linearized inversion. The clay volume is as a function of three random variables (K_{m}, G_{m}, and ρ_{m}), and the water saturation is as a function of two random variables (K_{fl} and ρ_{fl}). For illustration purposes, we show the derivation of the integration domain for water saturation.

For a given value of s_{w}, we solve the inequality $g(K_{\text{fl}}, \rho_{\text{fl}}) \le s_{\text{w}}$, assuming that the function g is the inverse of equations 27 and 28:

$$\frac{\frac{1}{K_{\text{fl}}} - \frac{1}{K_{\text{hc}}}}{\frac{1}{K_{\text{w}}} - \frac{1}{K_{\text{hc}}}} \le s_{\text{w}}, \tag{B-2}$$

$$\frac{\rho_{\text{fl}} - \rho_{\text{hc}}}{\rho_{\text{w}} - \rho_{\text{hc}}} \le s_{\text{w}}, \tag{B-3}$$

and we obtain

$$K_{\text{fl}} \le \frac{1}{s_{\text{w}}\left(\frac{1}{K_{\text{w}}} - \frac{1}{K_{\text{hc}}}\right) + \frac{1}{K_{\text{hc}}}} = c_1, \tag{B-4}$$

$$\rho_{\text{fl}} \le s_{\text{w}}(\rho_{\text{w}} - \rho_{\text{hc}}) + \rho_{\text{hc}} = c_2, \tag{B-5}$$

assuming $K_{\text{w}} \ge K_{\text{hc}}$ and $\rho_{\text{w}} \ge \rho_{\text{hc}}$. Therefore, the domain $D_{s_{\text{w}}}(K_{\text{fl}}, \rho_{\text{fl}}) = (-\infty, c_1] \times (-\infty, c_2]$. However, because the water saturation cannot be lower than zero, the lower limit of the fluid bulk modulus is K_{hc} (for $s_{\text{w}} = 0$) and the lower limit of the fluid density is ρ_{hc} (for $s_{\text{w}} = 0$). Hence, the domain $D_{s_{\text{w}}}(K_{\text{fl}}, \rho_{\text{fl}}) = [K_{\text{hc}}, c_1] \times [\rho_{\text{hc}}, c_2]$, with $K_{\text{hc}} \le c_1 \le K_{\text{w}}$ and $\rho_{\text{hc}} \le c_2 \le \rho_{\text{w}}$.

Similarly, we can derive the integration domain $D_{v_{\text{c}}}(K_{\text{m}}, G_{\text{m}}, \rho_{\text{fl}})$ for the clay volume. For a given value of v_{c}, we solve the inequality $g(K_{\text{m}}, G_{\text{m}}, \rho_{\text{m}}) \le v_{\text{c}}$ assuming that the function g is the inverse of equations 24–26 (notice that equations 24 and 25 lead to quadratic inequalities), and we obtain

$$K_{\text{m}} \ge \frac{1}{2}\left(v_{\text{c}}K_{\text{c}} + (1-v_{\text{c}})K_{\text{q}} + \frac{1}{v_{\text{c}}/K_{\text{c}} + (1-v_{\text{c}})/K_{\text{q}}}\right) = d_1, \tag{B-6}$$

$$G_m \geq \frac{1}{2}\left(v_c G_c + (1-v_c)G_q + \frac{1}{v_c/G_c + (1-v_c)/G_q}\right) = d_2, \tag{B-7}$$

$$\rho_m \geq v_c\rho_c + (1-v_c)\rho_q = d_3, \tag{B-8}$$

by assuming $K_c \leq K_q$, $G_c \leq G_q$, and $\rho_c \leq \rho_q$ and discarding the negative solutions. Therefore, we obtain that the domain $D_{v_c}(K_m, G_m, \rho_{fl}) = [d_1, +\infty) \times [d_2, +\infty) \times [d_3, +\infty)$. Because the clay volume cannot be greater than one, we obtain that the domain $D_{v_c}(K_m, G_m, \rho_{fl}) = [d_1, K_q] \times [d_2, K_q] \times [d_3, K_q]$, with $K_c \leq d_1 \leq K_q, G_c \leq d_2 \leq G_q$, and $\rho_c \leq d_3 \leq \rho_q$.

REFERENCES

Aki, K., and P. G. Richards, 1980, Quantitative seismology: W. H. Freeman & Co.

Avseth, P., T. Mukerji, and G. Mavko, 2005, Quantitative seismic interpretation: Cambridge University Press.

Ball, V., J. P. Blangy, C. Schiott, and A. Chaveste, 2014, Relative rock physics: The Leading Edge, **33**, 276–286, doi: 10.1190/tle33030276.1.

Berryman, J. G., 1999, Origin of Gassmann's equations: Geophysics, **64**, 1627–1629, doi: 10.1190/1.1444667.

Bosch, M., T. Mukerji, and E. F. Gonzalez, 2010, Seismic inversion for reservoir properties combining statistical rock physics and geostatistics: A review: Geophysics, **75**, no. 5, 75A165–75A176, doi: 10.1190/1.3478209.

Buland, A., and H. Kolbjørnsen, 2012, Bayesian inversion of CSEM and magnetotelluric data: Geophysics, **77**, no. 1, E33–E42, doi: 10.1190/geo2010-0298.1.

Buland, A., O. Kolbjørnsen, R. Hauge, Ø. Skjæveland, and K. Duffaut, 2008, Bayesian lithology and fluid prediction from seismic prestack data: Geophysics, **73**, no. 3, C13–C21, doi: 10.1190/1.2842150.

Buland, A., and H. Omre, 2003, Bayesian linearized AVO inversion: Geophysics, **68**, 185–198, doi: 10.1190/1.1543206.

Coléou, T., F. Allo, R. Bornard, J. Hamman, and D. Caldwell, 2005, Petrophysical seismic inversion: 75th Annual International Meeting, SEG, Expanded Abstracts, 1355–1358.

Connolly, P. A., and M. J. Hughes, 2016, Stochastic inversion by matching to large numbers of pseudo-wells: Geophysics, **81**, no. 2, M7–M22, doi: 10.1190/geo2015-0348.1.

Doyen, P. M., 2007, Seismic reservoir characterization: EAGE.

Doyen, P. M., and L. D. Den Boer, 1996, Bayesian sequential Gaussian simulation of lithology with non-linear data: U.S. Patent 5,539,704.

Dvorkin, J., M. Gutierrez, and D. Grana, 2014, Seismic reflections of rock properties: Cambridge University Press.

Eidsvik, J., P. Avseth, H. Omre, T. Mukerji, and G. Mavko, 2004, Stochastic reservoir characterization using prestack seismic data: Geophysics, **69**, 978–993, doi: 10.1190/1.1778241.

Gouveia, W.P., and J.A. Scales, 1998, Bayesian seismic waveform inversion: Parameter estimation and uncertainty analysis: Journal of Geophysical Research, **103**, 2759–2779, doi: 10.1029/97JB02933.

Grana, D., 2016, Bayesian linearized rock-physics inversion: Geophysics, **81**, no. 6, D625–D641, doi: 10.1190/geo2016-0161.1.

Grana, D., and E. Della Rossa, 2010, Probabilistic petrophysical-properties estimation integrating statistical rock physics with seismic inversion: Geophysics, **75**, no. 3, O21–O37, doi: 10.1190/1.3386676.

Grana, D., T. Fjeldstad, and H. Omre, 2017, Bayesian Gaussian mixture linear inversion for geophysical inverse problems: Mathematical Geosciences, **49**, 1–37, doi: 10.1007/s11004-016-9658-6.

Gray, F., T. Chen, and W. Goodway, 1999, Bridging the gap: Using AVO to detect changes in fundamental elastic constants: 69th Annual International Meeting, SEG, Expanded Abstracts, 852–855.

Gunning, J., and M. Glinsky, 2007, Detection of reservoir quality using Bayesian seismic inversion: Geophysics, **72**, no. 3, R37–R49, doi: 10.1190/1.2713043.

Hammer, H., O. Kolbjørnsen, H. Tjelmeland, and A. Buland, 2012, Lithology and fluid prediction from prestack seismic data using a Bayesian model with Markov process prior: Geophysical Prospecting, **60**, 500–515, doi: 10.1111/j.1365-2478.2011.01012.x.

Han, D., 1986, Effects of porosity and clay content on acoustic properties of sandstones and unconsolidated sediments: Ph.D. thesis, Stanford University.

Jullum, M., and O. Kolbjørnsen, 2016, A Gaussian based framework for Bayesian inversion of geophysical data to rock properties: Geophysics, **81**, no. 3, R75–R87, doi: 10.1190/geo2015-0314.1.

Kemper, M., and J. Gunning, 2014, Joint impedance and facies inversion: Seismic inversion redefined: First Break, **32**, 89–95.

Liu, M., and D. Grana, 2017, Stochastic seismic and petrophysical inversion using an ensemble-based method and data reparameterization: 87th Annual International Meeting, SEG, Expanded Abstracts, 3092–3096.

Mavko, G., and T. Mukerji, 1995, Seismic pore space compressibility and Gassmann's relation: Geophysics, **60**, 1743–1749, doi: 10.1190/1.1443907.

Mavko, G., T. Mukerji, and J. Dvorkin, 2009, The rock physics handbook: Cambridge University Press.

Mukerji, T., A. Jørstad, P. Avseth, G. Mavko, and J. R. Granli, 2001, Mapping lithofacies and pore-fluid probabilities in a North Sea reservoir: Seismic inversions and statistical rock physics: Geophysics, **66**, 988–1001, doi: 10.1190/1.1487078.

Murphy, W. F., III, 1984, Acoustic measures of partial gas saturation in tight sandstones: Journal of Geophysical Research, **89**, 11549–11559, doi: 10.1029/JB089iB13p11549.

Nur, A., 1992, Critical porosity and the seismic velocities in rocks: EOS, Transactions American Geophysical Union, **73**, 43–66.

Oldenburg, D., T. Scheuer, and S. Levy, 1983, Recovery of the acoustic impedance from reflection seismograms: Geophysics, **48**, 1318–1337, doi: 10.1190/1.1441413.

Osdal, B., O. Husby, H. A. Aronsen, N. Chen, and T. Alsos, 2006, Mapping the fluid front and pressure buildup using 4D data on Norne field: The Leading Edge, **25**, 1134–1141, doi: 10.1190/1.2349818.

Papoulis, A., 1984, Probability, random variables and stochastic processes: McGraw-Hill.

Rimstad, K., and H. Omre, 2010, Impact of rock-physics depth trends and Markov random fields on hierarchical Bayesian lithology/fluid prediction: Geophysics, **75**, no. 5, R93–R108, doi: 10.1190/1.3463475.

Russell, B., 1988, Introduction to seismic inversion methods: SEG.

Russell, B., 2013, A Gassmann-consistent rock physics template: CSEG Recorder, **38**, 23–30.

Russell, B., D. Gray, and D. P. Hampson, 2011, Linearized AVO and poroelasticity: Geophysics, **76**, no. 3, C19–C29, doi: 10.1190/1.3555082.

Sayers, C., and S. Chopra, 2009, Introduction to this special section: Seismic modeling: The Leading Edge, **28**, 528–529, doi: 10.1190/1.3124926.

Sen, M. K., and P. L. Stoffa, 1996, Bayesian inference, Gibbs sampler and uncertainty estimation in geophysical inversion: Geophysical Prospecting, **44**, 313–350, doi: 10.1111/j.1365-2478.1996.tb00152.x.

Sen, M. K., and P. L. Stoffa, 2013, Global optimization methods in geophysical inversion: Cambridge University Press.

Steffensen, I., and P. I. Karstad, 1995, Norne field development: Fast track from discovery to production: Journal of Petroleum Technology, **48**, 296–339, doi: 10.2118/30148-JPT.

Stolt, R. H., and A. B. Weglein, 1985, Migration and inversion of seismic data: Geophysics, **50**, 2458–2472, doi: 10.1190/1.1441877.

Suman, A., and T. Mukerji, 2013, Sensitivity study of rock physics parameters for modeling time-lapse seismic response of Norne field: Geophysics, **78**, no. 6, D511–D523, doi: 10.1190/geo2013-0045.1.

Tarantola, A., 2005, Inverse problem theory: SIAM.

Tjelmeland, H., and H. Omre, 1997, A complex sand-shale facies model conditioned on observations from wells, seismic and production, *in* E. Y. Baafi and N. A. Shofield, eds., Geostatistics Wollongong 1996: Kluwer Academic Publishers, 634–646.

Ulvmoen, M., and H. Omre, 2010, Improved resolution in Bayesian lithology/fluid inversion from prestack seismic data and well observations. Part 1: Methodology: Geophysics, **75**, no. 2, R21–R35, doi: 10.1190/1.3294570.

Ulrych, T. J., M. D. Sacchi, and A. Woodbury, 2001, A Bayes tour of inversion: A tutorial: Geophysics, **66**, 55–69, doi: 10.1190/1.1444923.